In situ selectivity profiling and crystal structure of SML-8-73-1, an active site inhibitor of oncogenic K-Ras G12C

John C. Hunter[a], Deepak Gurbani[a], Scott B. Ficarro[b,c], Martin A. Carrasco[a], Sang Min Lim[b,d,e], Hwan Geun Choi[b,d], Ting Xie[e], Jarrod A. Marto[b,c], Zhe Chen[f], Nathanael S. Gray[b,d], and Kenneth D. Westover[a,1]

[a]Departments of Biochemistry and Radiation Oncology and [f]Department of Biophysics, University of Texas Southwestern Medical Center at Dallas, Dallas, TX 75390, [b]Department of Cancer Biology and [c]Blais Proteomics Center, Dana–Farber Cancer Institute, Boston, MA 02115; [d]Department of Biological Chemistry and Molecular Pharmacology, Harvard Medical School, Boston, MA 02115; and [e]Department of Chemistry and Chemical Biology, Harvard University, Cambridge, MA 02138

Edited* by Roger D. Kornberg, Stanford University School of Medicine, Stanford, CA, and approved May 12, 2014 (received for review March 12, 2014)

Directly targeting oncogenic V-Ki-ras2 Kirsten rat sarcoma viral oncogene homolog (K-Ras) with small-molecule inhibitors has historically been considered prohibitively challenging. Recent reports of compounds that bind directly to the K-Ras G12C mutant suggest avenues to overcome key obstacles that stand in the way of developing such compounds. We aim to target the guanine nucleotide (GN)-binding pocket because the natural contents of this pocket dictate the signaling state of K-Ras. Here, we characterize the irreversible inhibitor SML-8-73-1 (SML), which targets the GN-binding pocket of K-Ras G12C. We report a high-resolution X-ray crystal structure of G12C K-Ras bound to SML, revealing that the compound binds in a manner similar to GDP, forming a covalent linkage with Cys-12. The resulting conformation renders K-Ras in the open, inactive conformation, which is not predicted to associate productively with or activate downstream effectors. Conservation analysis of the Ras family GN-binding pocket reveals variability in the side chains surrounding the active site and adjacent regions, especially in the switch I region. This variability may enable building specificity into new iterations of Ras and other GTPase inhibitors. High-resolution in situ chemical proteomic profiling of SML confirms that SML effectively discriminates between K-Ras G12C and other cellular GTP-binding proteins. A biochemical assay provides additional evidence that SML is able to compete with millimolar concentrations of GTP and GDP for the GN-binding site.

CPM assay | ActivX

Multiple lines of evidence suggest that if achievable, inhibiting V-Ki-ras2 Kirsten rat sarcoma viral oncogene homolog (K-Ras) signaling may have therapeutic advantages in cancer. Approximately 30% of all human cancers contain activating Ras mutations, making them one of the most common identifiable molecular drivers of cancer (1, 2). K-Ras mutation–positive tumors tend to be less responsive to current therapy than other biological subtypes, and patients with these tumors have worse cancer outcomes (3, 4). We aim to develop and evaluate direct-acting inhibitors of K-Ras as a therapeutic strategy.

Ras proteins are GTPase enzymes that transduce extracellular signals when growth factors bind to extracellular receptors, resulting in cellular responses such as proliferation, apoptosis, and differentiation (5). Activating signals are transmitted when Ras is bound to GTP and cease once the bound GTP is hydrolyzed to GDP. Two structurally dynamic loops, so-called "switch I" (residues 25–40 in K-Ras) and "switch II" (residues 57–75 in K-Ras) form a key portion of the binding interface between K-Ras and a number of regulators and downstream effectors, including Raf kinases, PI3 kinases, and RalGDS (6–8). We hypothesize that to be successful, direct-acting K-Ras inhibitors must alter the conformation of switch I and/or switch II such that it becomes incapable of transmitting activating signals. Because the guanine nucleotide (GN)-binding pocket dictates the switch conformation, we postulate that developing compounds binding to this region will have a high likelihood of modulating K-Ras signaling.

Development of GN competitive inhibitors of K-Ras is challenging because GTP and GDP bind with subnanomolar affinity and intracellular concentrations of GTP and GDP are high. Recently, our group (9) and Shokat and coworkers (10) independently developed and reported two classes of compounds that have a direct impact on productive nucleotide binding to the GN-binding site. Both target a common activating mutation, G12C, to achieve irreversible binding. K-Ras G12C is present in an estimated 10–20% of Ras-driven cancers and in roughly 50% of Ras-mutated lung adenocarcinomas (11–13). For lung cancer alone, this means that therapeutics targeting the G12C mutation could treat roughly 25,000 people per year in the United States (14). Mutations at codon 12, along with the other most common cancer-causing Ras mutations at codons 13 and 61, decrease intrinsic GTPase activity to some extent and impair interactions with GTPase-activating proteins that modulate (GTP) hydrolysis. Codon 12 is adjacent to the active site, such that the mutation places a solvent-accessible cysteine near the GN terminal phosphate.

Significance

SML-8-73-1 (SML) is the first example, to our knowledge, of a GTP-competitive inhibitor of V-Ki-ras2 Kirsten rat sarcoma viral oncogene homolog (K-Ras). A high-resolution structure of K-Ras G12C bound to SML shows K-Ras in an inactive conformation. In situ proteomic-based chemical profiling of SML demonstrates that SML is highly selective for K-Ras G12C over other small GTPases. A novel chemosensor-based assay allows measurement of covalent reaction rates between K-Ras G12C and SML and enables characterization of this reaction in the context of millimolar concentrations of GTP and GDP, well in exccss of what is found in living cells. These results demonstrate that even in the presence of high concentrations of GTP and GDP, SML is able to exchange into the GN site.

Author contributions: J.C.H., S.B.F., M.A.C., S.M.L., H.G.C., T.X., J.A.M., N.S.G., and K.D.W. designed research; J.C.H., D.G., S.B.F., M.A.C., H.G.C., T.X., J.A.M., Z.C., N.S.G., and K.D.W. performed research; S.B.F., S.M.L., H.G.C., T.X., J.A.M., and N.S.G. contributed new reagents/analytic tools; J.C.H., D.G., S.B.F., J.A.M., Z.C., N.S.G., and K.D.W. analyzed data; and J.C.H. and K.D.W. wrote the paper.

The authors declare no conflict of interest.

*This Direct Submission article had a prearranged editor.

Data deposition: The atomic coordinates and structure factors have been deposited in the Protein Data Bank, www.pdb.org (PDB ID codes 4OBE, 4LDJ, and 4NMM).

[1]To whom correspondence should be addressed. E-mail: kenneth.westover@utsouthwestern.edu.

This article contains supporting information online at www.pnas.org/lookup/suppl/doi:10.1073/pnas.1404639111/-/DCSupplemental.

We previously reported development of SML-8-73-1 (SML), a GDP analog containing an electrophilic warhead extending from the beta-phosphate that undergoes a Michael reaction addition to Cys-12, forming a stable thioether linkage (9). Even in the presence of large excesses of GDP and GTP, quantitative complete irreversible binding was observed by MS. In biochemical assays, SML prevents K-Ras association with the Ras-binding domain of the downstream effector BRaf. Preliminary cellular tests using a cell-permeable caged prodrug version, SML-10-70-1, demonstrated that treatment of a G12C mutant K-Ras cancer cell line with the SML class of compounds, albeit at a high concentration (100 μM), leads to inactivation of K-Ras and down-regulation of Akt and Erk signaling pathways, demonstrating as a proof of concept that the GN-binding pocket is a viable target for inhibitors of Ras signaling.

Here, we provide three lines of evidence to support further the concept of targeting the GN-binding pocket of K-Ras. First, we report high-resolution X-ray crystal structures of K-Ras, including a structure containing the irreversible inhibitor, SML, bound to K-Ras G12C. The models are analyzed with the aim of understanding implications for K-Ras interactions with downstream effectors. Second, we address compound selectivity with MS-based in situ profiling demonstrating that SML preferentially interacts with K-Ras G12C over most other cellular GTP-binding proteins. Finally, we provide additional evidence that in a purified system, SML is able to compete for the GN-binding site of K-Ras G12C in the presence of millimolar concentrations of GTP and GDP, similar to those found in a living cell. The prospects for developing GTPase inhibitors are also broadly considered.

Results

X-Ray Structures of K-Ras. Three high-resolution X-ray crystal structures of K-Ras in two different crystal forms were solved: (*i*) WT K-Ras bound to GDP (1.2 Å, C2 space group), (*ii*) G12C K-Ras bound to GDP (1.1 Å, $P2_12_12_1$ space group), and (*iii*) G12C K-Ras bound to SML (1.9 Å, $P2_12_12_1$ space group) using molecular replacement with Protein Data Bank (PDB) ID code 4EPV (15) as the search model (Table S1). The structure of GDP-bound G12C K-Ras is highly similar to the WT structure (rmsd of ∼0.33 Å) and to previously reported K-Ras structures, including PDB ID codes 4EPV, 4EPR (15), 4L9S, 4LPK (10), and 4DSU (16). Unlike prior G12C structures, the switch I and switch II regions are well ordered and oriented in an open conformation consistent with structures of GDP-bound WT K-Ras and H-Ras. The G12C structure is nearly identical to the WT K-Ras with respect to the protein main chain but reveals clear electron density for the Cys-12 side chain extending down from the P-loop toward the terminal phosphate from bound GDP. This orientation is geometrically compatible with a Michael reaction between the sulfur of the cysteine and the chloroacetamide group of our covalent inhibitor SML (Fig. 1).

To obtain crystals of SML-bound K-Ras, we incubated the protein with a 10-fold molar excess of compound at 37 °C for 2 h to achieve ∼95% labeled protein as determined by MS (Fig. S1). The crystals grew in the same space group and unit cell dimensions as GDP-bound G12C and diffracted to 1.89 Å. Following molecular replacement with a ligand-free model, we observed density in the GN-binding pocket consistent with the presence of SML (Fig. 1*C*). We also noted additional Fo-Fc density around Cys-12, indicating that the side chain of Cys-12 adopts an alternate conformation, rotated ∼100° away from the GN pocket, an orientation not observed in our GDP-bound G12C structure. The density around the GN-binding site was similar to that of GDP but showed continuous positive density connecting the beta-phosphate to the rotated conformation of Cys-12, consistent with the presence of SML in the GN pocket and a covalent linkage between Cys-12 and SML. Therefore we

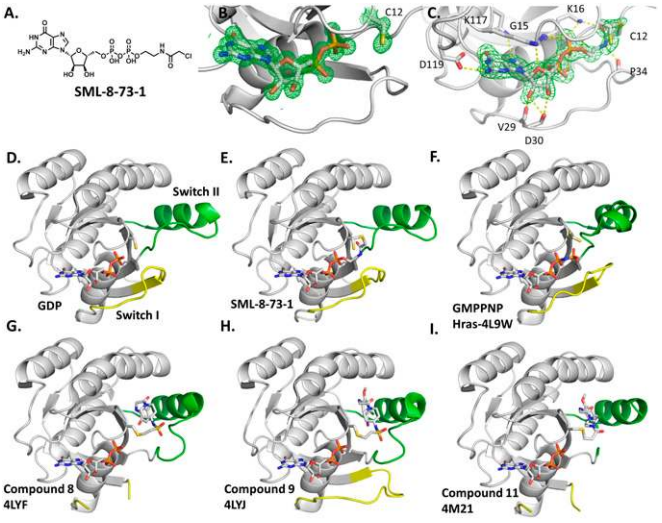

Fig. 1. Structures of K-Ras G12C. (*A*) Chemical structure of SML. (*B*) Structure of K-Ras G12C bound to GDP. A 2Fo-Fc map contoured at 1.1 sigma is displayed for GDP and the Cys-12 side chain, and it shows a separation between the ligand and side chain. (*C*) Structure of K-Ras G12C bound to SML. An Fo-Fc omit map contoured at 2.5 sigma shows the inhibitor in the GN-binding site and density extending to Cys-12. Interactions between the ligand and protein are shown by yellow dashed lines. (*D–I*) Cys-12–binding compounds alter the conformation of switches I and II. X-ray crystal structures of GDP-bound (inactive) G12C K-Ras (*D*) and guanosine 5′-[β,γ-imido] triphosphate (GMPPNP, a nonhydrolyzable GTP analog)-bound G12C Ras (*F*, 4L9W) are shown for comparison, with switch I colored yellow and switch II colored green. (*E*) When bound to SML, G12C K-Ras assumes a conformation nearly identical to GDP-bound G12C K-Ras, with both switch regions in the inactive conformation (rmsd of ∼0.17 Å). (*G–I*) Structures of G12C K-Ras bound to type III covalent inhibitors reported by Shokat and coworkers (10) demonstrate alternative conformations of both switch regions apparently induced by interactions between residues 58 and 62 and the type III inhibitors causing a change in switch I, which is observed in *H* but is disordered in *G* and *I*.

modeled 50% of the Cys-12 side chain in the rotated alternative conformation, forming a covalent linkage with the terminal carbon atom of SML, and 50% in the previously observed conformation to fit the Fo-Fc density (Fig. 1*A*).

A comparison of the SML-bound structure with the GDP-bound structure confirms that both switch I and switch II are in the inactive, open conformation (Fig. 1 *D–F*). Both Tyr-32 and Thr-35, which rotate toward the active site in the presence of GTP upon Ras activation (PDB ID code 3GFT), are rotated away, whereas the other switch I residues assume a conformation nearly identical to that of the GDP-bound form. SML is in an orientation similar to that of GDP with extensive contacts to multiple residues in the GN pocket (Fig. 1 *B* and *C*). Additionally, the carbonyl oxygen and amide nitrogen of SML are within hydrogen bonding distance of Lys-16 and the main-chain carbonyl oxygen of Pro-34, respectively (Fig. 1*C*).

Comparison with Switch II Pocket-Binding Compounds. Recently, another class of Cys-12–modifying K-Ras inhibitors was reported, which access Cys-12 not from the nucleotide pocket, as is observed for SML, but instead bind to an inhibitor-induced pocket adjacent to switch II and Cys-12, which has been named the switch II pocket (SII-P) (10). Functionally, these compounds cause an ∼100-fold decrease in the affinity of the enzyme for GTP relative to GDP, leading to a decrease in the total level of activated mutant K-Ras. Conceptually, these compounds are similar to non ATP-competitive, "type III" kinase inhibitors (17). As opposed to type I and II kinase inhibitors, which compete with ATP for binding, type III inhibitors do not compete with ATP and have

been observed to bind simultaneously with ATP (18). In the same spirit, we will refer to the non-GN competitive inhibitors as type III Ras inhibitors and to the nucleoside-competitive inhibitors as type I Ras inhibitors.

Previously reported crystal structures of type III inhibitors bound to K-Ras demonstrate that binding of these compounds results in a rearrangement of both the switch I and switch II regions into an orientation that was never previously observed (10) (Fig. 1 *G–I*). This appears to be caused by interactions between the switch II residues Thr-58 and Asp-62 with the type III inhibitors, which reorder the switch II region and lead to destabilization of switch I so that it moves away from the GN pocket. In addition, the magnesium is absent in a number of the inhibitor-bound structures, consistent with rearrangement of switch I and significant reordering or destabilization of the GN-binding site.

Predicted impact of SML on Ras signaling. K-Ras transduces signals when bound to GTP by directly binding to downstream effector proteins. Therefore, we anticipate that an effective inhibitor of K-Ras signaling must efficiently disrupt this interaction. We superimposed the structure of SML-bound K-Ras with previously solved structures of Ras-effector (Raf1 and PI3K) complexes to predict whether SML-bound K-Ras exhibits a conformation that would be predicted to have productive interactions with these effectors.

Based on prior structures, switch I is the main interface between Ras and PI3K and Raf1. The H-Ras/Raf1 complex (PDB ID code 4G0N) demonstrates that Tyr-32 and Thr-35 rotate to coordinate with the gamma-phosphate of the non-hydrolysable GTP-mimetic, GMPPNP, constraining the orientation of residues D33, I36, S39, and R41 to allow interactions with residues 64–69, 84, and 88–89 on Raf. Similarly, the Ras/PI3K structure (PDB ID code 1HE8) (7) shows that with GTP binding, residues 36–41 of the switch I region rotate to interact with residues 221–234 and residues 251–258 from PI3K and lead to activation of PI3K (Fig. 2 *A* and *B*). The conformation of switch I found in the SML structure is incompatible with either binding mode observed in the Ras/effector complexes (Fig. 2 *C* and *D*).

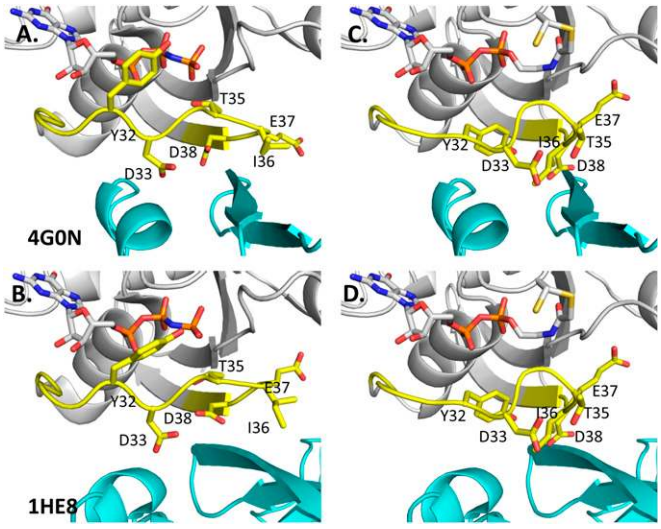

Fig. 2. SML-bound K-Ras G12C is unlikely to engage downstream effector proteins. The interface for the Ras/Raf (*A*) and Ras/PI3K (*B*) complexes as observed by X-ray crystallography (PDB ID codes 4G0N and 1HE8) are displayed with Ras shown in gray (with the switch I region colored yellow) and Raf and PI3K shown in cyan. In both of these structures, residues 33, 36, and 38 from switch I swing out to form interactions with Raf and PI3K. (*C* and *D*) SML-bound structure of G12C K-Ras was superimposed onto GMPPNP/Ras as in *A* and *B*. When bound to the SML inhibitor, the previously mentioned side chains from switch I have changed conformation. The SML-induced conformation of switch I is not compatible with Raf or PI3K interactions, as previously observed, because of clashes.

Conservation of the GN-binding site and implications for development of specific K-Ras inhibitors. Achieving specificity will be essential for developing GN-binding inhibitors of K-Ras or other small GTPases due to the large number of GDP/GTP-binding proteins within the cell (Ras dendrogram in Fig. S2). To understand the prospects for developing specific inhibitors of K-Ras family members better, we studied the conservation of the GN-binding site and SII-P residues with the hypothesis that variability in these residues would translate into different topologies in the GN and SII-P sites, which could be used to make future compounds with differential selectivity across the family. This hypothesis has been previously tested directly through kinase inhibitor profiling experiments, which indicate that sequence conservation can predict the feasibility of making selective inhibitors (19).

We performed a multiple sequence alignment on 160 Ras superfamily members using the Clustal-Omega multiple sequence alignment tool (20–22). We then processed these alignments using a structural conservation analysis program, ConSurf, to generate relative conservation scores for each residue in the K-Ras sequence (23–26). This algorithm calculates relative conservation scores for each residue that are then normalized so that the average score across all residues is zero. As a rough guide to our data, the range of scores spanned from about −2.5 to 2.5, with lowest score representing the most highly conserved residues and the highest score representing the most variable residues.

Residues within 4 Å of the inhibitor were selected for initial study, based on the assumption that residues within 4 Å would be accessible to small-molecule inhibitors occupying either the GN-binding site or the S-IIP site. We added to this segment any residues that lay within one or two residues of interacting amino acids to define block segments. Using this approximation, we identified five sequence segments that interact with SML and four segments that interact with the S-IIP site (Fig. 3). The mean conservation score of each of these segments, based on the normalized scores obtained from the ConSurf analysis, was calculated. Of the SML segments, the switch I region (residues 28–34) was the most variable, with a score of 0.003, whereas the region behind switch II (residues 58–59) showed the highest degree of conservation, with a score of −1.233. For the S-IIP, residues 60–63 were best conserved, with a score of −0.853, and the region near the top of the S-IIP region (residues 96–100) showed the most variability, with a score of −0.166. As an aggregate estimate of the relative conservation of the SML vs. S-IIP sites, we calculated the overall average conservation scores. The scores of both regions were similar, with scores of −0.762 and −0.557 and with an average variability of 10.4 and 11.4 amino acids per position for the GN and S-IIP sites, respectively.

Kinases serve as a relevant point of reference for this analysis because a number of potent and highly selective protein kinase inhibitors have been developed despite an ATP-binding site that is generally well conserved (27). Incidentally, at the outset of kinase inhibitor development, some assumed that this conservation would prevent development of selective inhibitors (28, 29). Kinase inhibitor selectivity has been achieved, first, because a range of chemical scaffolds, most of which do not resemble ATP, have been identified and, second, because many compounds occupy a binding pocket adjacent to the ATP binding site that is less well conserved. As a comparison, we performed the same conservation analysis on a subset of 210 kinases, which included three arms of the kinome, including the cAMP-dependent, cGMP-dependent, and protein kinase C (AGC) protein kinase family; the cyclin-dependent kinases, mitogen-activated protein kinases, glycogen synthase kinases, and CDK-like kinases (CMGC) protein kinase family; and the tyrosine kinase family in an effort to anticipate the relative difficulty of achieving selective GTPase inhibitors compared with selective kinase inhibitors. Using an

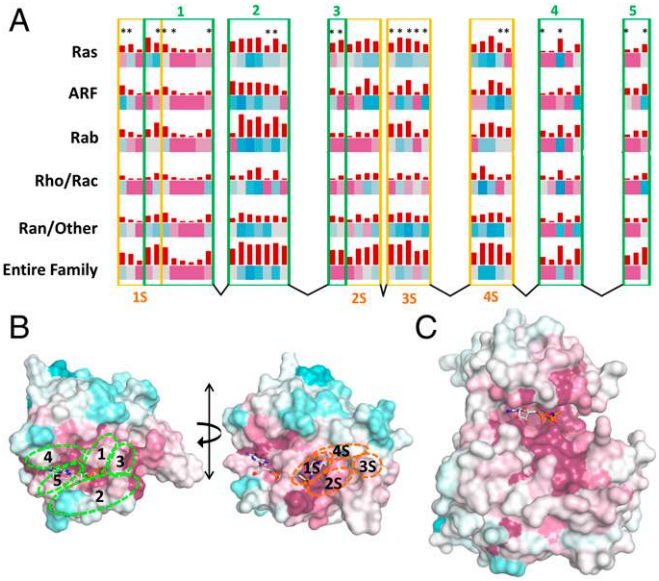

Fig. 3. Conservation analysis of amino acids surrounding the GN-binding site. (*A*) Amino acid level conservation. Protein sequences for each small GTPase subfamily, including the Ras family, ADP ribosylation factor (ARF) family, Ras-related proteins in brain (Rab) family, Rho/Rac family, and the Ras-related nuclear protein (Ran) family, or for the entire Ras superfamily, were aligned using the Clustal-Omega multiple sequence alignment server, and relative conservation scores for each amino acid were calculated using the ConSurf server. Residues within 4 Å of either SML or switch II pocket (SIIP)-binding compound 9 (10) (PDB ID code 4LYJ) based on crystal structures were selected as residues with potential to interact with compounds and highlighted in green or orange, respectively. Relative conservation scores for these residues are represented in a blue (poorly conserved) to red (well-conserved) gradient. The variability at each position is depicted using a red bar above each amino acid position; the height is proportional to the number of different residues observed at each position in the subfamily. Positions where cysteines are observed in at least one Ras family member are marked with an asterisk. (*B* and *C*) Topology of amino acid conservation. (*B*) Conservation scores for the entire Ras family are plotted on the surface of the K-Ras G12C X-ray structure (PDB ID code 4LDJ). Regions within 4 Å of the compound-binding sites are highlighted as above. (*C*) Relative conservation of each amino acid across 210 kinases is plotted on the 3D structure of spleen tyrosine kinase (SYK) (52) (PDB ID code 4FL1). The regions surrounding the GN-binding site and SIIP binding site of K-Ras are less well conserved (average conservation scores of −0.762, −0.557, and 10.4: 11.4 amino acids per position, respectively) than the regions surrounding the kinase ATP-binding site (average conservation score of −1.43 and 8.3 residues per position).

approach similar to that described above, we aligned and generated conservation scores for these serine/threonine and tyrosine kinases. Again, amino acid positions within 4 Å of the ATP-binding site were selected for study, and the average conservation score was calculated for these regions.

A visual representation of the conservation scores projected onto the structures K-Ras and a typical kinase fold show that the ATP-binding pocket is highly conserved across these kinase families, with the ATP-interacting residues exhibiting an overall relative conservation score of −1.43, with an average variability of 8.3 amino acids per position, which is slightly more conserved than the relative level of conservation seen in the GN-binding pocket of Ras family members, −0.762, with an average variability of 10.4 amino acids per position. If sequence conservation is a valid predictor of the potential to achieve compound selectivity, this analysis suggests that relative to kinase inhibitors, there should be more options for achieving specificity with compounds targeting the GN-binding site and neighboring regions.

***In situ* MS-based GTPase profiling of SML.** We wondered if targeting Cys-12 with covalent chemistry, independent of other modifications to distinguish SML-class compounds from GDP, was sufficient to confer selectivity for K-Ras G12C over other GN-binding proteins. Our prior work demonstrated that SML selectively interacts with the G12C mutant K-Ras over WT protein (9), and we hypothesized that the covalent nature of SML would provide a high degree of selectivity across a broad set of GN-binding proteins. To test this empirically, the compound was profiled at a concentration of 100 μM utilizing MIA PaCa-2 lysates (a human pancreatic carcinoma cell line homozygous for the K-Ras G12C mutation) using ActivX technology (ActivX Biosciences, Inc.) (30, 31). This approach measures the ability of test compounds, such as SML, to protect a subset of GTP-binding proteins from labeling with a lysine-reactive GTP-biotin probe and is similar to technology commonly used to profile kinase inhibitors. In our MIA PaCa cell lysates, over 100 different GTP-binding proteins were detectable. SML was able to inhibit probe labeling for K-Ras G12C significantly after 15 min of incubation at a concentration of 100 μM in gel-filtered cell lysates. Moderate inhibition of probe labeling was seen for three other GTP-binding proteins, only one of which is a small GTPase (full profiling data are available in Table 1 and Table S2). The profiling data are also important because they confirm that the electrophilic warhead of SML is sufficiently stable and selective to function in a context similar to the intracellular milieu. However, because this technique involves a gel filtration step that removes small molecules from the protein fraction before compound incubation, this experiment is unable to address the question of whether SML can efficiently compete in the context of high concentrations of GTP and GDP.

SML efficiently competes with GTP and GDP for binding to G12C-K-Ras. Overcoming the millimolar intracellular concentration of GDP/GTP is a significant challenge in the development of GN pocket-targeted Ras inhibitors that bind efficiently to K-Ras. To assess the potential of SML to compete with GNs, we developed a chemosensor assay to measure the rate of covalent bond formation. For this assay, we used a cysteine-reactive compound, 7-diethylamino-3-(4-maleimidophenyl)-4-methylcoumarin, or CPM, which exhibits negligible fluorescence until reaction with a thiol group. This compound efficiently reacts with Cys-12 of GN-bound mutant K-Ras to yield an ∼10-fold higher fluorescent signal than seen with WT GN-bound K-Ras. Following covalent addition of SML to Cys-12, however, the thiol is no longer available to react with CPM, and the fluorescent signal drops to that of WT K-Ras.

We used this assay to measure the rate of reaction between SML and G12C K-Ras in the presence and absence of 1.5 mM GDP and 1.5 mM GTP (200-fold excess over SML) (Fig. 4). Of note, even in the "absence" of GN, the inhibitor must displace GDP, which remains bound to the K-Ras active site through purification steps, as evidenced by the X-ray structure of K-Ras G12C, which shows the active site occupied by GDP; protein used for these crystals was never exposed to supplemental GDP or GTP before crystallization. The results demonstrate that the inhibitor is able to compete with a large excess of GDP for GN site binding, albeit at a decreased rate compared with samples without an excess of GN ($t_{1/2}$ of 0.7 h vs. 12 h). However, despite

Table 1. Proteins showing inhibition of GTP-biotin labeling by SML

Protein	Family	Inhibition, %
K-Ras G12C	Small GTPase, Ras	82.9
EFTUD1	GTP-binding elongation factor	73.3
GUF1	GTP-binding elongation factor	72.6
ARL3	Small GTPase, Arf	65.1

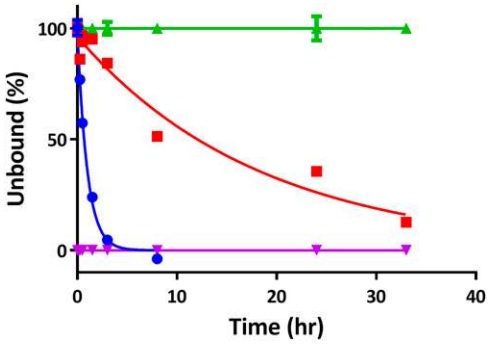

Fig. 4. SML efficiently competes with GTP and GDP for binding to G12C KRas. A thiol-reactive compound, CPM, exhibits a dramatic increase in fluorescence following reaction with Cys-12, leading to a significant increase in signal for G12C (green) relative to WT (purple) K-Ras. This assay was used to determine the rate of covalent reaction between K-Ras Cys-12 and SML in the absence (blue) or presence of 1.5 mM GTP and GDP (red).

the slower rate, these data unambiguously demonstrate that SML is able to compete irreversibly, preventing GN from exchanging back in. This suggests that a covalent inhibitor may be able to overcome the endogenous pool of GDP/GTP within the cell due to the relatively long 14- to 24-h $t_{1/2}$ of Ras if appropriate dosing regimens can be developed that maintain exposure of G12C K-Ras to covalent inhibitors (32, 33). We note that this assay method will be useful in developing inhibitors of K-Ras G12C with more "drug-like" characteristics, and it also may be applied to other protein targets for which cysteine-targeted irreversible therapeutics are being developed.

Discussion

Although multiple attempts to generate Ras-targeted therapies have been reported, most notably targeting farnesyl transferase, none of these has yielded clinically useful drugs (34). A number of strategies are under investigation, including further attempts to inhibit the C-terminal processing of Ras by prenyltransferases, the proteolytic enzyme Ras-converting enzyme, and the methyltransferase isoprenylcysteine-carboxyl-methyltransferase (35, 36). Recently, small molecules that compete for the prenyl-binding site of PDEδ, a protein that regulates the spatial distribution of K-Ras in cells, were also reported as another potential direct therapeutic strategy (37). Nevertheless, the difficulties with direct Ras targeting have led many to focus on other factors upstream and downstream in the Ras signaling pathways, including EGF receptor, Raf, MEK, and PI3 kinases. These efforts have seen mixed results, and combination therapies with inhibitors targeting multiple pathways may be necessary for optimal benefit (38–40). The best therapeutic strategies for addressing Ras dysregulation in cancer, be they direct or indirect, remain unclear. We have focused our attention on developing GTP competitive inhibitors because the GN-binding site is adjacent to switches I and II, which mediate most interactions between Ras and its effectors. We therefore anticipate that developing compounds occupying this site will have the potential to modulate Ras signaling pathways.

Ultimately, for this effort to succeed, compounds must have (*i*) the capacity to perturb biological systems in a way that is therapeutically advantageous, (*ii*) sufficient selectivity to target cancer-related Ras proteins over other GTP-binding proteins involved in normal cellular processes, and (*iii*) sufficient potency to overcome high concentrations of cellular GTP and GDP. In this study, we have provided additional evidence that SML, in principle, meets these specifications. We have also provided support for generalization of this approach to other GTPases.

Structural studies of Ras family members have largely focused on H-Ras until recently. Over the past 2 y, 25 structures of K-Ras have become available as renewed enthusiasm for targeting K-Ras has grown, highlighted by a recently announced National Cancer Institute initiative that will focus specifically on development of methods to inhibit K-Ras directly for therapeutic purposes. In total, seven different crystal forms have been observed, and structures of a number of oncogenic mutations, including G12D, G12V, G12C, and Q61H, have been reported. With this report, we have added to this growing collection of data by solving high-resolution structures of K-Ras in three relevant forms, including a G12C oncogenic form bound to GDP in which both switch regions are well ordered, as well as a structure of our covalent K-Ras inhibitor, SML, bound to the G12C mutant of K-Ras. The cocrystal structure demonstrates that SML-bound K-Ras G12C is locked in an inactive conformation that would not be predicted to interact productively with Ras effector proteins, consistent with our prior biochemical characterization (9).

It should be noted that the switch regions are dynamic, as evidenced by the many switch conformations observed in the multitude of available Ras crystal structures. However, when bound to GTP, switch I and II assume a distinct closed conformation that favors interaction with Raf and other signal mediators. Therefore, to disrupt this interaction, it is presumably only necessary for the inhibitor to prevent Ras from assuming the active conformation. In other words, there is no requirement to achieve one specific inactive conformation; there may be many inactive conformations that can be achieved with a range of different inhibitor scaffolds targeting the GN-binding pocket and surrounding regions that will likely have the same inhibitory effect on Ras signaling. We therefore speculate that although binding of SML to K-Ras G12C places the protein in a conformation that is known to be inactive, a number of other approaches may also achieve the goal of impairing Ras signaling (41).

SML provides a proof of principle that a covalent compound can both compete with GDP and GTP for the GN-binding site of K-Ras and exhibit a high degree of specificity. We anticipate that this concept may allow targeting of other small GTPases as well. For example, with respect to cancer, it might be useful to develop inhibitors against Rac and Rho family members, because Rac and Rho are often overexpressed in cancer cells to support altered tumor physiology (42–44). Indeed, it has been shown that misregulation of Rac and Rho signaling leads to disruption of junctions and actin cytoskeleton reorganization, allowing cancer cell migration and invasion (45). Non-Ras GTPases have also been implicated in cell cycle progression, through regulation of cyclin D3 and NF-κB signaling pathways (46, 47). Our sequence analysis of Ras family GTPases demonstrates that a number of these contain cysteine residues near the GN-binding site that may be amenable to cysteine-targeted irreversible inhibition (residues marked by asterisks in Fig. 3*A* and specific GTPases listed in Table S3). Another general option for targeting the active site of GTPases would be to aim for the conserved lysine K16, which is a conserved residue that becomes covalently bound to the ActivX probe.

The use of covalent inhibitors for therapeutic purposes has many precedents. Nevertheless, despite the fact that there are ~40 US Food and Drug Administration (FDA)-approved covalent drugs on the market, including widely used and effective compounds such as 2-acetoxybenzoic acid (aspirin), penicillin, proton pump inhibitors, and clopidogrel (Plavix), there has traditionally been reluctance by the industry to develop compounds containing reactive moieties. Nonspecific interactions between strongly electrophilic warheads and nontarget proteins in the blood and in cells, leading to acute tissue damage, haptenization of proteins, and activation of immune responses, have been cited as reasons (48). It should be noted that compounds, such as

aspirin and penicillin, were not designed to be covalent but were simply observed to act through a covalent mechanism. Therefore, the prior reluctance to develop targeted covalent inhibitors may relate less to the absolute potential usefulness of covalent therapeutics and more to a general lack of expertise that would be required to design safe and effective covalent drugs systematically. It is becoming clearer that toxicity concerns may be manageable by careful compound design and optimization of electrophile reactivity (49). The recent emergence of several FDA-approved covalent kinase inhibitors, including Ibrutinib and Afatinib, suggests that the methods and technology for rationally designing covalent inhibitors have matured to the point that they may be broadly applicable (50, 51). As a general method, the chemosensor assay presented here may be of particular use in optimizing the relative reactivity of electrophilic functional groups and kinetics of covalent inhibition of various targets due to the efficiency with which a large number of samples and time points can be monitored inexpensively and in a high-throughput format.

The potential advantages often cited for covalent drugs include better potency, selectivity, and effective $t_{1/2}$ compared with noncovalent drugs (48). With respect to K-Ras inhibitors, the advantages also appear to extend to overcoming high-affinity interactions between K-Ras and its natural nucleotide ligands and more effectively competing with the high concentration of endogenous nucleotide in the cell.

Methods

SML was synthesized as reported previously (9). Protein expression and purification, and liquid chromatography-electrospray ionization-MS of intact K-Ras G12C were also performed as reported previously (9). Detailed descriptions of all other methods, including X-ray crystallography, the CPM assay, sequence conservation analysis, and MS-based chemical profiling are provided in *SI Methods*.

ACKNOWLEDGMENTS. This work was supported by CPRIT Grant R1207 (to K.D.W.) and Grant I1829 from The Welch Foundation (to K.D.W.). Results shown in this report are derived from work performed at the Structural Biology Center at the Advanced Photon Source, Argonne National Laboratory. The Argonne National Laboratory is operated by UChicago Argonne, LLC, for the US Department of Energy, Office of Biological and Environmental Research, under Contract DE-AC02-06CH11357.

1. Bos JL (1989) ras oncogenes in human cancer: A review. *Cancer Res* 49(17):4682–4689.
2. Prior IA, Lewis PD, Mattos C (2012) A comprehensive survey of Ras mutations in cancer. *Cancer Res* 72(10):2457–2467.
3. Eberhard DA, et al. (2005) Mutations in the epidermal growth factor receptor and in KRAS are predictive and prognostic indicators in patients with non-small-cell lung cancer treated with chemotherapy alone and in combination with erlotinib. *J Clin Oncol* 23(25):5900–5909.
4. Lièvre A, et al. (2008) KRAS mutations as an independent prognostic factor in patients with advanced colorectal cancer treated with cetuximab. *J Clin Oncol* 26(3):374–379.
5. Ellis CA, Clark G (2000) The importance of being K-Ras. *Cell Signal* 12(7):425–434.
6. Scheffzek K, et al. (1997) The Ras-RasGAP complex: Structural basis for GTPase activation and its loss in oncogenic Ras mutants. *Science* 277(5324):333–338.
7. Pacold ME, et al. (2000) Crystal structure and functional analysis of Ras binding to its effector phosphoinositide 3-kinase gamma. *Cell* 103(6):931–943.
8. Wittinghofer A, Pai EF (1991) The structure of Ras protein: A model for a universal molecular switch. *Trends Biochem Sci* 16(10):382–387.
9. Lim SM, et al. (2014) Therapeutic targeting of oncogenic K-Ras by a covalent catalytic site inhibitor. *Angew Chem Int Ed Engl* 53(1):199–204.
10. Ostrem JM, Peters U, Sos ML, Wells JA, Shokat KM (2013) K-Ras(G12C) inhibitors allosterically control GTP affinity and effector interactions. *Nature* 503(7477):548–551.
11. Forbes SA, et al. (2011) COSMIC: Mining complete cancer genomes in the Catalogue of Somatic Mutations in Cancer. *Nucleic Acids Res* 39(Database issue):D945–D950.
12. Greulich H, et al. (2012) Functional analysis of receptor tyrosine kinase mutations in lung cancer identifies oncogenic extracellular domain mutations of ERBB2. *Proc Natl Acad Sci USA* 109(36):14476–14481.
13. Jones S, et al. (2004) Increased frequency of the k-ras G12C mutation in MYH polyposis colorectal adenomas. *Br J Cancer* 90(8):1591–1593.
14. Stephen AG, Esposito D, Bagni RK, McCormick F (2014) Dragging ras back in the ring. *Cancer Cell* 25(3):272–281.
15. Sun Q, et al. (2012) Discovery of small molecules that bind to K-Ras and inhibit Sos-mediated activation. *Angew Chem Int Ed Engl* 51(25):6140–6143.
16. Maurer T, et al. (2012) Small-molecule ligands bind to a distinct pocket in Ras and inhibit SOS-mediated nucleotide exchange activity. *Proc Natl Acad Sci USA* 109(14):5299–5304.
17. Garuti L, Roberti M, Bottegoni G (2010) Non-ATP competitive protein kinase inhibitors. *Curr Med Chem* 17(25):2804–2821.
18. Spicer JA, et al. (2007) 4-anilino-5-carboxamido-2-pyridone derivatives as non-competitive inhibitors of mitogen-activated protein kinase kinase. *J Med Chem* 50(21):5090–5102.
19. Knight ZA, Lin H, Shokat KM (2010) Targeting the cancer kinome through polypharmacology. *Nat Rev Cancer* 10(2):130–137.
20. Wennerberg K, Rossman KL, Der CJ (2005) The Ras superfamily at a glance. *J Cell Sci* 118(Pt 5):843–846.
21. Sievers F, et al. (2011) Fast, scalable generation of high-quality protein multiple sequence alignments using Clustal Omega. *Mol Syst Biol* 7:539.
22. Goujon M, et al. (2010) A new bioinformatics analysis tools framework at EMBL-EBI. *Nucleic Acids Res* 38(Web Server issue):W695–W699.
23. Ashkenazy H, Erez E, Martz E, Pupko T, Ben-Tal N (2010) ConSurf 2010: Calculating evolutionary conservation in sequence and structure of proteins and nucleic acids. *Nucleic Acids Res* 38(Web Server issue):W529–W533.
24. Celniker G, et al. (2013) ConSurf: Using evolutionary data to raise testable hypotheses about protein function. *Isr J Chem* 53(3-4):199–206.
25. Landau M, et al. (2005) ConSurf 2005: The projection of evolutionary conservation scores of residues on protein structures. *Nucleic Acids Res* 33(Web Server issue):W299–W302.
26. Glaser F, et al. (2003) ConSurf: Identification of functional regions in proteins by surface-mapping of phylogenetic information. *Bioinformatics* 19(1):163–164.
27. Fabbro D, Cowan-Jacob SW, Möbitz H, Martiny-Baron G (2012) Targeting cancer with small-molecular-weight kinase inhibitors. *Methods Mol Biol* 795:1–34.
28. Lawrence DS, Niu J (1998) Protein kinase inhibitors: The tyrosine-specific protein kinases. *Pharmacol Ther* 77(2):81–114.
29. Toledo LM, Lydon NB, Elbaum D (1999) The structure-based design of ATP-site directed protein kinase inhibitors. *Curr Med Chem* 6(9):775–805.
30. Patricelli MP, et al. (2007) Functional interrogation of the kinome using nucleotide acyl phosphates. *Biochemistry* 46(2):350–358.
31. Patricelli MP, et al. (2011) In situ kinase profiling reveals functionally relevant properties of native kinases. *Chem Biol* 18(6):699–710.
32. Magee AI, Gutierrez L, McKay IA, Marshall CJ, Hall A (1987) Dynamic fatty acylation of p21N-ras. *EMBO J* 6(11):3353–3357.
33. Bergo MO, et al. (2004) Inactivation of Icmt inhibits transformation by oncogenic K-Ras and B-Raf. *J Clin Invest* 113(4):539–550.
34. Adjei AA, et al. (2003) Phase II study of the farnesyl transferase inhibitor R115777 in patients with advanced non-small-cell lung cancer. *J Clin Oncol* 21(9):1760–1766.
35. Wang W, Fang G, Rudolph J (2012) Ras inhibition via direct Ras binding—Is there a path forward? *Bioorg Med Chem Lett* 22(18):5766–5776.
36. Gysin S, Salt M, Young A, McCormick F (2011) Therapeutic strategies for targeting ras proteins. *Genes Cancer* 2(3):359–372.
37. Zimmermann G, et al. (2013) Small molecule inhibition of the KRAS-PDEδ interaction impairs oncogenic KRAS signalling. *Nature* 497(7451):638–642.
38. Nissan MH, Rosen N, Solit DB (2013) ERK pathway inhibitors: How low should we go? *Cancer Discov* 3(7):719–721.
39. Rinehart J, et al. (2004) Multicenter phase II study of the oral MEK inhibitor, CI-1040, in patients with advanced non-small-cell lung, breast, colon, and pancreatic cancer. *J Clin Oncol* 22(22):4456–4462.
40. Roberts PJ, Stinchcombe TE, Der CJ, Socinski MA (2010) Personalized medicine in non-small-cell lung cancer: Is KRAS a useful marker in selecting patients for epidermal growth factor receptor-targeted therapy? *J Clin Oncol* 28(31):4769–4777.
41. Burns MC, et al. (2014) Approach for targeting Ras with small molecules that activate SOS-mediated nucleotide exchange. *Proc Natl Acad Sci USA* 111(9):3401–3406.
42. Alan JK, Lundquist EA (2013) Mutationally activated Rho GTPases in cancer. *Small GTPases* 4(3):159–163.
43. Mack NA, Whalley HJ, Castillo-Lluva S, Malliri A (2011) The diverse roles of Rac signaling in tumorigenesis. *Cell Cycle* 10(10):1571–1581.
44. Fritz G, Kaina B (2006) Rho GTPases: Promising cellular targets for novel anticancer drugs. *Curr Cancer Drug Targets* 6(1):1–14.
45. O'Connor K, Chen M (2013) Dynamic functions of RhoA in tumor cell migration and invasion. *Small GTPases* 4(3):141–147.
46. Rathinam R, Berrier A, Alahari SK (2011) Role of Rho GTPases and their regulators in cancer progression. *Front Biosci (Landmark Ed)* 16:2561–2571.
47. Villalonga P, Ridley AJ (2006) Rho GTPases and cell cycle control. *Growth Factors* 24(3):159–164.
48. Singh J, Petter RC, Baillie TA, Whitty A (2011) The resurgence of covalent drugs. *Nat Rev Drug Discov* 10(4):307–317.
49. Dahal UP, Obach RS, Gilbert AM (2013) Benchmarking in vitro covalent binding burden as a tool to assess potential toxicity caused by nonspecific covalent binding of covalent drugs. *Chem Res Toxicol* 26(11):1739–1745.
50. Advani RH, et al. (2013) Bruton tyrosine kinase inhibitor ibrutinib (PCI-32765) has significant activity in patients with relapsed/refractory B-cell malignancies. *J Clin Oncol* 31(1):88–94.
51. Miller VA, et al. (2012) Afatinib versus placebo for patients with advanced, metastatic non-small-cell lung cancer after failure of erlotinib, gefitinib, or both, and one or two lines of chemotherapy (LUX-Lung 1): A phase 2b/3 randomised trial. *Lancet Oncol* 13(5):528–538.
52. Gradler U, et al. (2013) Structural and biophysical characterization of the Syk activation switch. *J Mol Biol* 425(2):309–333.